Journal of Photochemistry & Photobiology, A: Chemistry 467 (2025) 116427

Contents lists available at ScienceDirect

Journal of Photochemistry & Photobiology, A: Chemistry

journal homepage: www.elsevier.com/locate/jphotochem

Photoreactivity of 1-azidostyrene and 3-phenyl-*2H*-azirine in acetonitrile and cryogenic matrices☆

W.Dinindu Mendis [a], Abdelqader M. Jamhawi [b], Rajkumar Merugu [a], Dmitrii Govorov [a], Katrin H. Vilinsky [a], Bakar Alomari [a], Bruce S. Ault [a], A.Jean-Luc Ayitou [b], Anna D. Gudmundsdottir [a,*]

[a] Department of Chemistry, University of Cincinnati, PO Box 210172, Cincinnati OH 45221, United States
[b] Department of Chemistry, University of Illinois, Chicago IL 60607, United States

ARTICLE INFO

Keywords:
Vinyl azide
Vinylnitrene
Ketenimine
Argon matrix
2-methyltetrahydrofuran matrix
Laser flash photolysis
Ultrafast transient absorption spectroscopy

ABSTRACT

Despite their versatile synthetic utility, vinyl azides have complex and poorly understood photochemistry. To address this, we investigated the photoreactivity of 1-azidostyrene **1** and 3-phenyl-*2H*-azirine **2** in solution and cryogenic matrices. In argon matrices, irradiation of **1** at 254 nm yielded **2**, phenyl nitrile ylide **3**, and N-phenyl ketenimine **4**, whereas irradiation at wavelengths above 300 nm produced only **2** and **4**. Similarly, irradiation of **1** in 2-methyltetrahydrofuran (mTHF) glass at 77 K mainly yielded absorption corresponding to the formation of **2** (λ_{max} ~ 252 nm). In contrast, irradiation of **2** at wavelengths above 300 nm in Argon matrices yielded no photoproducts, whereas irradiation at 254 nm resulted in the formation of **3**. Furthermore, femto- and nano-second transient absorption and laser flash photolysis were performed to ascertain the transient species and reactive intermediates formed during the photochemical transformations of **1** and **2**. The ultrafast transient absorption spectroscopy of **1** resulted in a transient absorption band centered at ca. 472 nm with a time constant τ ~ 22 ps, which was assigned to the first singlet excited state (S_1) of **1**. The nano-second flash photolysis of **1** (308 nm laser) generated **2** within the laser pulse (~17 ns), and subsequently **2** is excited to yield triplet vinylnitrene ^{3}**1N** with an absorption centered at ~ 440 nm. In contrast, the nano-second laser flash photolysis of **2** with 266 nm laser produced a weak absorption corresponding to **3**, whereas 308 nm laser yielded absorption due to triplet vinylnitrene ^{3}**1N** (λ_{max} ~ 440 nm). These findings demonstrate that the direct irradiation of **1** populates S_1 of **1**, which does not intersystem cross to form ^{3}**1N**, but instead decays to yield **2**. Density functional theory calculations supported the characteristics of the excited states and reactive intermediates formed upon irradiation of **1** and **2**.

1. Introduction

Vinyl azides are versatile building blocks in organic synthesis and their ability to undergo 1,3-cycloaddition has been extensively used to synthesize diverse *N*-heterocycles [1–4]. Furthermore, the drive for more sustainable synthesis of valuable chemicals has led to light being used as a traceless/massless reagent to transform vinyl azide derivatives into heterocyclic compounds with varying degrees of structural complexity [5–7]. Furthermore, the photochemistry of azides has inspired interest in photoclick reactions to afford triazole scaffolds [8,9]. However, the photochemical transformations of vinyl azides are complex and not well understood. Upon excitation, vinyl azide derivatives can react in a concerted manner from a hot excited state or by forming singlet or triplet vinylnitrene intermediates [10].

It is documented that triplet vinylnitrenes can be formed photochemically from vinyl azide, azirine, or isoxazole derivatives [11]. For example, the irradiation of azirine derivatives with short-wavelength light causes C–C bond breakage, resulting in the formation of the corresponding ylides. In contrast, irradiation at longer wavelengths can induce C–N bond cleavage to form a triplet vinylnitrene, especially in azirines with a built-in triplet sensitizer. Similarly, the irradiation of vinyl azides with a built-in triplet sensitizer leads to triplet vinylnitrene formation [12]. However, the direct irradiation of vinyl azides yields the corresponding azirines, presumably through a concerted reaction from

☆ This article is part of a special issue entitled: 'George S. Hammond' published in Journal of Photochemistry & Photobiology, A: Chemistry.

* Corresponding author.
E-mail address: Anna.Gudmundsdottir@uc.edu (A.D. Gudmundsdottir).

https://doi.org/10.1016/j.jphotochem.2025.116427
Received 12 February 2025; Received in revised form 28 March 2025; Accepted 2 April 2025
Available online 3 April 2025

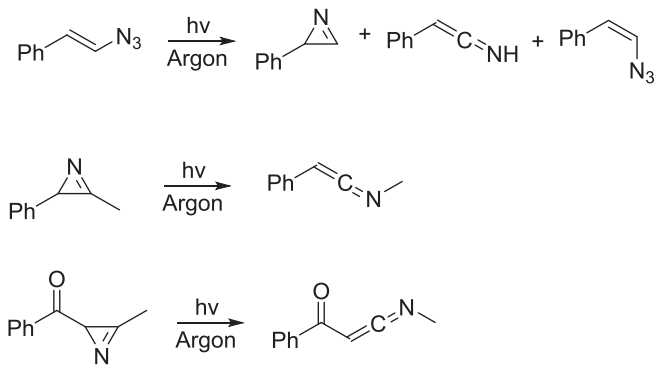

Scheme 1. Products formed by irradiating noncyclic vinyl azides and azirines in argon matrices [10,19,16].

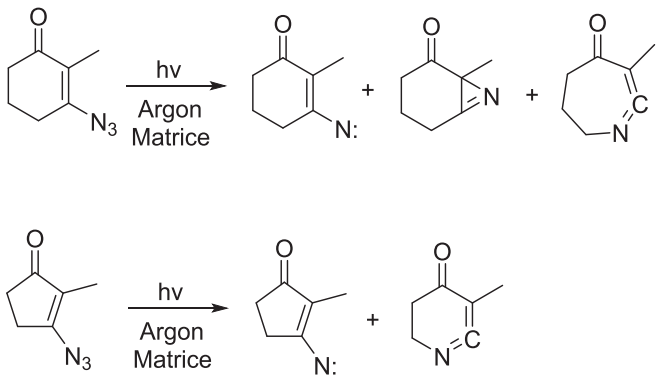

Scheme 2. Products formed by irradiation of cyclic vinyl azides in argon matrices [26].

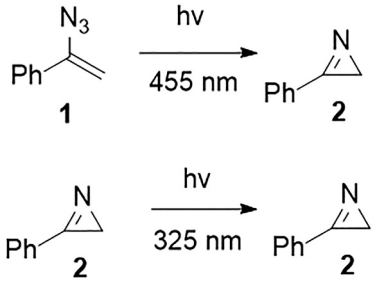

Scheme 3. Products formed upon irradiation of **1** in acetonitrile-d_3 using a 455 ± 10 nm LED and **2** in chloroform-*d* using IK3202R-D laser (325 nm) through a Pyrex filter.

the singlet excited state or through vinylnitrene formation [10,13,14]. Products analysis does not aid in elucidating the photoreaction mechanism of vinyl azides and azirines because azirine products can potentially be formed from both singlet or triplet excited states and singlet or triplet vinylnitrenes.

Triplet vinylnitrenes have been directly detected in solution using laser flash photolysis [15,12,16–19]. These intermediates are generally short-lived, decaying predominantly via intersystem crossing to form the corresponding azirines. This behavior contrasts with that of other triplet nitrenes stabilized by electron-donating substituents, such as alkyl- and arylnitrenes, which are typically long-lived in solution and decay by dimerization to form azo dimers [20–22]. In contrast, singlet vinylnitrenes have not yet been detected, although multiconfigurational calculations indicate that they are stable intermediates, with the open-shell singlet being more stable than the closed-shell singlet [23–25]. Notably, these calculations also suggest that triplet vinylnitrenes are more stable than their singlet configurations.

Although obtaining electron spin resonance and infrared (IR) spectra in cryogenic matrices is the most accurate method for identifying triplet vinylnitrenes, these intermediates are generally not stable under these conditions, which hinders characterization. For example, as shown in Scheme 1, upon irradiation in cryogenic matrices, simple noncyclic vinyl azides or azirines do not yield triplet vinylnitrenes, presumably because the vinylnitrene undergoing intersystem crossing to form the corresponding ketenimine or azirine [10,19,16].

Vinyl azides that are part of a cyclic structure can yield triplet vinylnitrenes that are stable at cryogenic temperatures (Scheme 2) [17,18,26]. The cyclic structure has been theorized to prevent rotation of the vinylnitrene moiety around the vinylic C=C bond, thereby hindering intersystem crossing and the formation of stable ground-state photoproducts [18].

In cryogenic matrices, cyclic vinylnitrenes are formed concurrently with ketenimine products [26]. Thus, vinylnitrenes are not precursors to the ketenimine derivatives. Instead, the ketenimines likely form directly from the excited state of the vinyl azides. Additionally, the conversion of triplet vinylnitrenes to the corresponding ketenimines can occur upon further irradiation or photochemically [17,26].

Pimentel and co-workers have shown that the direct irradiation of 1-azidostyrene (**1**) in cryogenic matrices does not yield the corresponding triplet vinylnitrene ^{3}**1N**, but rather 3-phenyl-*2H*-azirine **2** and N-phenyl ketenimine **4** as well as phenyl nitrile ylide **3** via secondary irradiation of **2** [27]. We theorized that an excited state of **1** forms **2** in a concerted manner, but it remains unclear whether **4** is formed from an excited state of **1** or via intersystem crossing of ^{3}**1N**. Thus, to clarify the mechanism of photoproduct formation, we investigated the photoreactivity of **1** in cryogenic matrices and acetonitrile. Specifically, we used ultrafast transient absorption spectroscopy to determine the fate of the first singlet excited state (S_1) of **1** and attempted to detect the formation of singlet vinylnitrene ^{1}**1N**. To aid in understanding the photoreactivity of **1**, we also investigated the photochemistry of **2** in cryogenic matrices and solution. Density functional theory (DFT) calculations (B3LYP/6–31 + G(d) and B3PW91/6–311 + G(d,p)) were used to support the characterization of the excited states and intermediates observed upon excitation of **1** and **2** as well as the proposed reactions mechanisms.

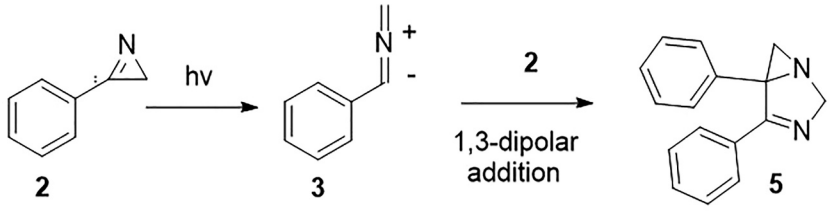

Scheme 4. Formation of **5** via **3** upon irradiation of **2** in chloroform-*d* through Pyrex.

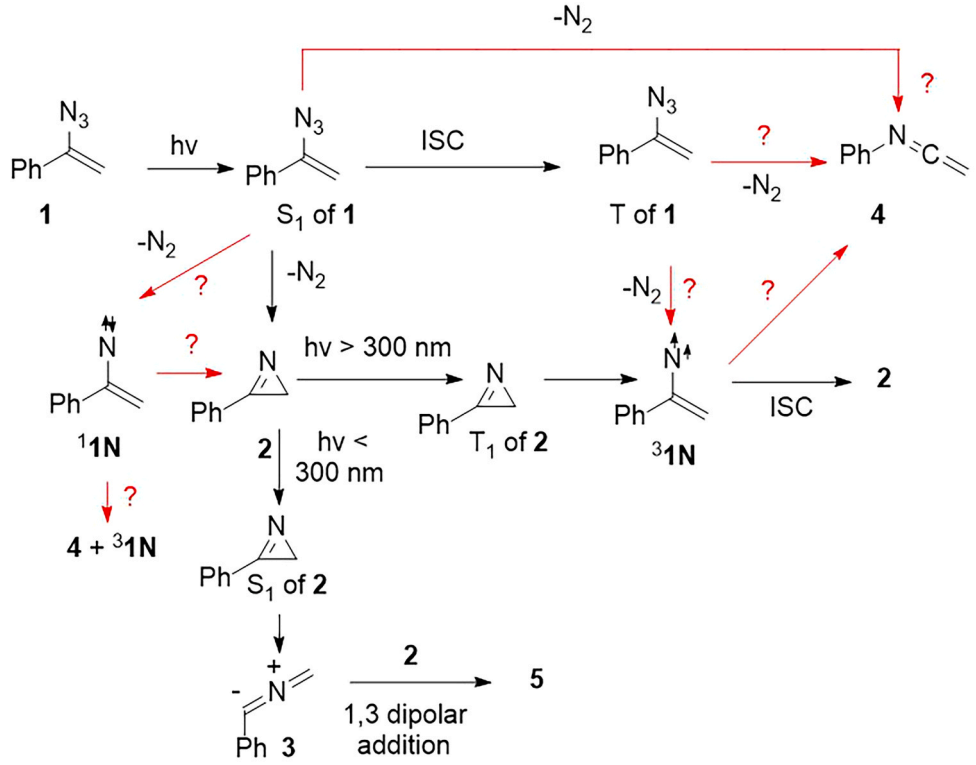

Scheme 5. Proposed mechanism for photoproduct formation upon irradiating **1** and **2** in acetonitrile and cryogenic matrices.

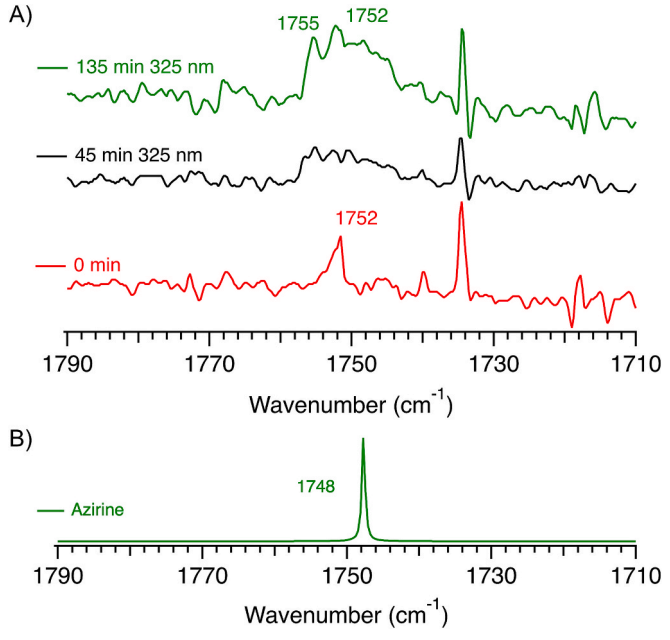

Fig. 1. A) Difference IR spectra were obtained by irradiating **1** in an Argon matrix at 14 K with a 325 nm laser for 45 and 135 min. B) IR spectrum of **2** calculated at the B3LYP level of theory with the 6–31+G(d) basis set and scaling by 0.9603.

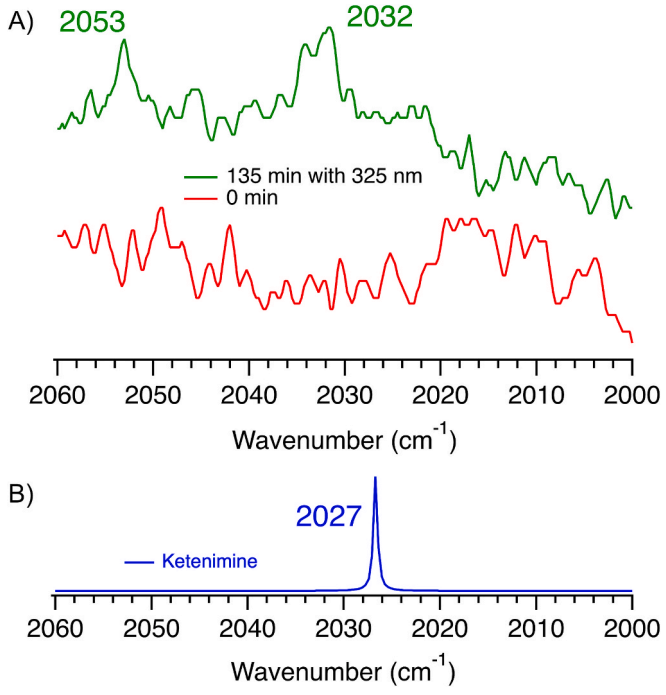

Fig. 2. A) Difference IR spectra obtained by irradiating **1** in an Argon matrix at 14 K with a 325 nm laser for 135 min. B) IR spectrum of **4** calculated at the B3LYP level of theory with the 6–31+G(d) basis set and scaling by 0.9603.

2. Materials and methods

2.1. Preparation of compounds

2.1.1. Synthesis of azide 1

Azide **1** was synthesized according to a previously described procedure [28–30]. 1,2-Dibromoethylbenzene (1.512 g, 5.73 mmol) was dissolved in dimethylformamide (15 mL); then, NaN_3 (1.11 g, 17.16 mmol) was added and the mixture was stirred overnight at room temperature. After reaction, the solution was diluted with distilled water (35 mL), and the organic material was extracted with diethyl ether (2 x

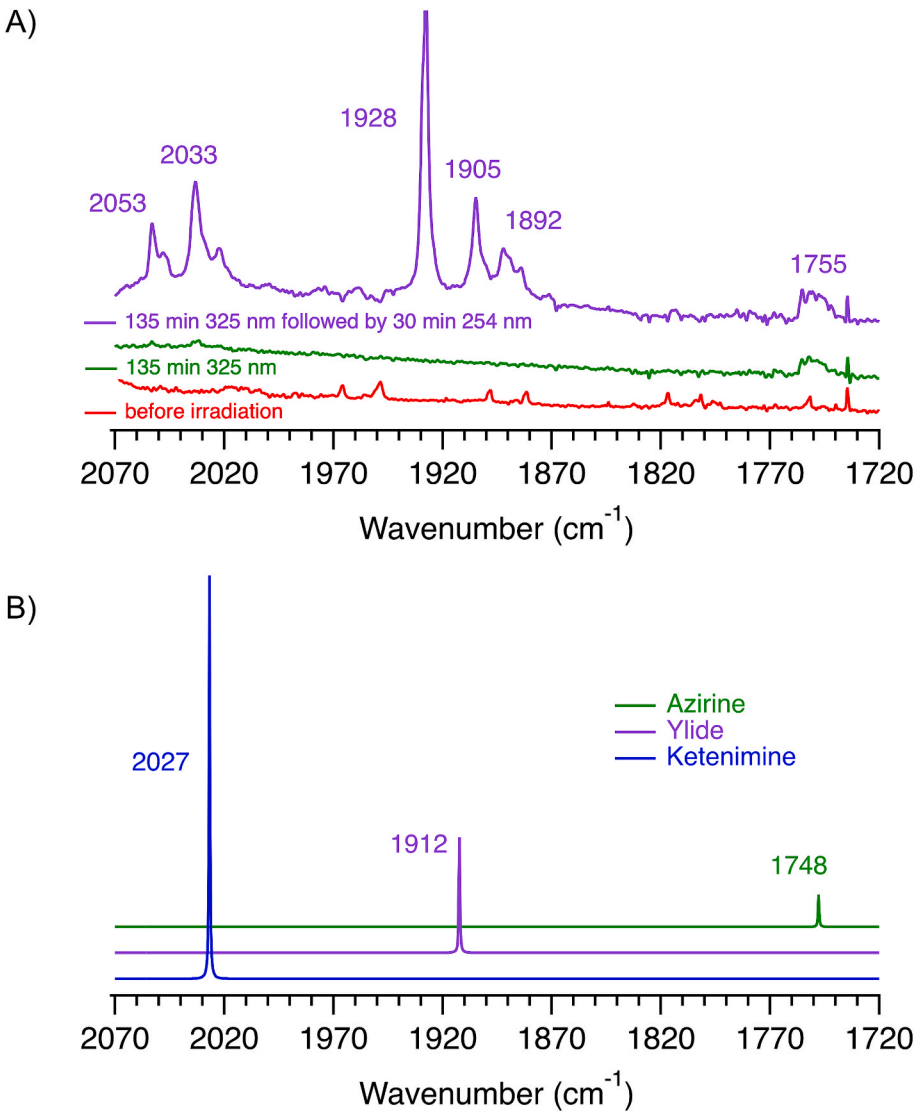

Fig. 3. A) Difference IR spectra (2070–1720 cm^{-1}) obtained by irradiating **1** in an Argon matrix at 14 K with a 325 nm laser for 135 min followed by a 254 nm UV pen for 30 min. B) IR spectra of **2**, **3**, and **4** calculated at the B3LYP level of theory with the 6–31+G(d) basis set and scaling by 0.9603.

35 mL). The combined organic fraction was washed with distilled water (3 x 25 mL) and dried over *anh.* $MgSO_4$. Following solvent evaporation under vacuum, the crude residue was purified using flash column chromatography over silica gel using a solvent system of hexanes:EtOAc (99:1 v/v) to obtain the expected azide **1** (594 mg, 4.09 mmol, 71 % yield). Azide **1** was further characterized using NMR and FTIR spectroscopy; the obtained spectra were consistent with reported data [28,30,29].

^{1}H NMR (400 MHz, $CDCl_3$): δ 7.56 (dd, J = 6.6, 2.8 Hz, 2H), 7.36 (dd, J = 5.3, 1.8 Hz, 3H), 5.43 (d, J = 2.4 Hz, 1H), 4.96 (d, J = 2.4 Hz, 1H) ppm. ^{13}C NMR (101 MHz, $CDCl_3$): δ 145.0, 134.3, 129.1, 128.5, 125.57, 98.0 ppm. FTIR (neat): 2108, 1636, 1260, 1019, 930, 798, 747, 692 cm^{-1}.

2.1.2. Synthesis of azirine 2

Following a literature procedure [4], **2** was synthesized by photolyzing **1**. Azide **1** (40.7 mg, 0.35 mmol) was dissolved in acetonitrile-d_3 (1.00 mL) in a Pyrex NMR tube. After sealing the tube with a rubber septum, the reaction solution was slowly purged with Argon for 20 min. Subsequently, the solution was irradiated with a blue LED light (455 nm) for 4 days [4]. ^{1}H NMR and FTIR spectroscopy revealed quantitative formation of azirine **2** (46.8 mg, 0.32 mmol, 91 % yield); the obtained spectra corresponded well with reported data [29,28].

^{1}H NMR (400 MHz, $CDCl_3$): δ 7.93–7.90 (m, 2H), 7.62–7.54 (m, 3H), 1.80 (s, 2H) ppm. FTIR (neat): 2917, 2849, 1737, 1678, 1447, 1240, 1003, 757, 694 cm^{-1}.

2.1.3. Photolysis of azirine 2

Azirine **2** (2 mg, 0.017 mmol) was dissolved in $CDCl_3$ (0.6 mL) in a NMR tube. The reaction solution was purged with Argon for 8 min, and the tube was sealed with a rubber septum. The tube/solution was irradiated using a mercury arc lamp housed in Pyrex cooling jacket for 135 min. The photoreaction of **2** was monitored using ^{1}H NMR spectroscopy, which showed the formation of the expected 4,5-diphenyl-1,3-diazabicyclo[3.1.0]hex-3-ene **5** [31].

^{1}H NMR (400 MHz, $CDCl_3$): δ 7.71–7.69 (m, 2H), 7.40–7.27 (m, 8H), 5.23 (d, 1H) 4.94 (d, 1H) 3.01 (s, 1H) 1.82 (s, 1H) ppm. ^{13}C NMR (101 MHz, $CDCl_3$): δ 172.2, 136.2, 132.0, 130.8, 129.2, 128.92, 128.86, 128.44, 128.31, 84.8, 60.1, 39.3 ppm. FTIR(neat): 3358, 2924, 1610, 1330, 996, 691, 554 cm^{-1}. GCMS (EI): 234 (M^+), 233 (100).

2.1.4. Preparative photolysis to form 5

Azide **1** (27 mg, 0.19 mmol) was dissolved in benzene (30 mL) in a Pyrex flask. The reaction solution was purged with Argon for 10 min,

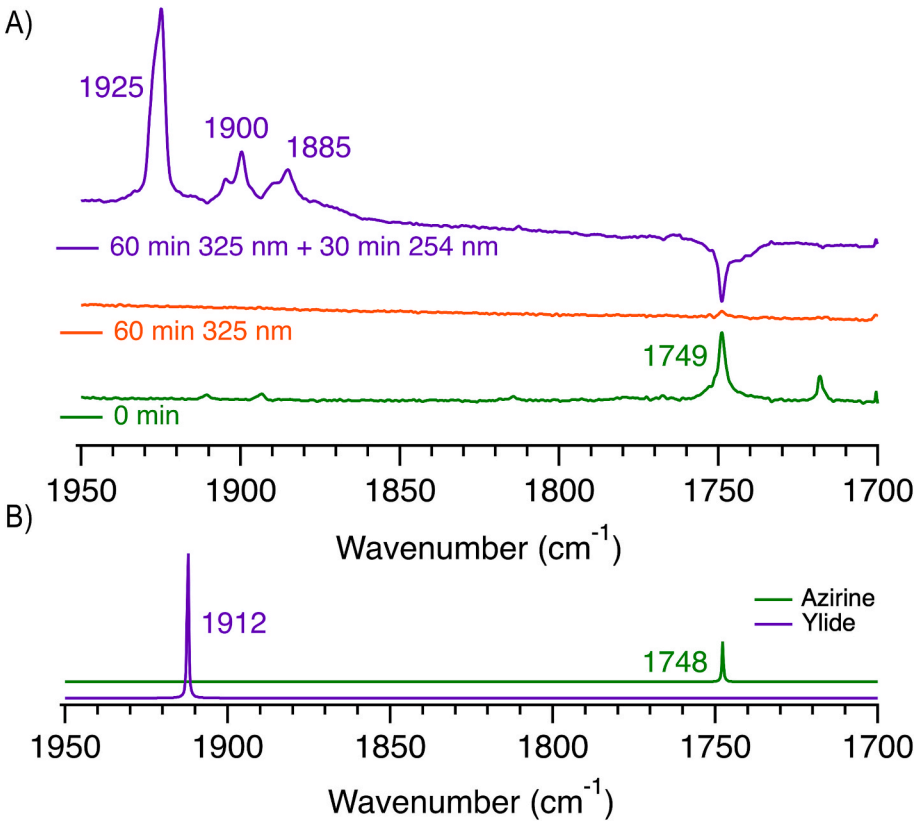

Fig. 4. A) Difference IR spectra (1950–1700 cm^{-1}) obtained by irradiating **2** in an argon matrix at 14 K with a 325 nm laser for 60 min followed by a 254 nm UV pen for 30 min. B) IR spectra of **2** and **3** calculated using the B3LYP level of theory with the 6–31+G(d) basis set and scaling by 0.9603.

and the flask was sealed with a rubber septum. The reaction flask was irradiated using a mercury arc lamp housed in Pyrex cooling jacket for 10 h. The photoreaction of **1** was monitored using ^{1}H NMR spectroscopy, which showed the formation of the expected 4,5-diphenyl-1,3-diazabicyclo[3.1.0]hex-3-ene **5** and only traces remaining **1** or **2**. The crude reaction mixture (20 mg, 0.085 mmol, 90 % yield) was purified using silica gel column chromatography to yield **5** (11 mg, 0.047 mmol, 50 % yield).

2.2. Uv–vis spectroscopy in glassy 2-methyltetrahydrofuran (mTHF) matrices

The photoreactivity of azide **1** in mTHF glass at 77 K was investigated using UV–vis absorption spectroscopy instrument equipped with a temperature-controlled cryostat as described previsouly.[32] A solution of azide **1** (5 μL) in anhydrous mTHF was prepared so that the maximum absorbance was less than 1.0. The sample (2 mL) was transferred into a temperature-resistant 10 mm × 10 mm quartz cuvette, which was then inserted into the sample holder. After the outer and inner chambers were vacuum-sealed, liquid nitrogen was poured into the cryostat to achieve an interior temperature of 77 K that froze the sample solution into a glassy matrix. The absorption spectrum of **1** in the mTHF glass was recorded over specific time periods while the matrix was irradiated using a Xe lamp (quartz), with and without a Pyrex filter (ca. 300 nm cutoff).

2.3. IR spectroscopy in argon matrices

Matrix isolation of **1** or **2** was performed using a conventional argon matrix isolation setup [33]. Argon was deposited at 14 K on a cold CsI window. Azide **1** was sublimed at 313 K and deposited with an argon flow at 14 K for 2 h under vacuum. For azirine **2**, a deposition time of 3 h was used to obtain a better spectrum. The matrix was irradiated with an IK3202R-D laser (325 nm) or Hg-UV pen (254 nm).

2.4. Laser flash photolysis

Laser flash photolysis was performed using a Nd:YAG laser (266 or 354 nm, 2–3 ns) or excimer laser (308 nm, ~ 17 ns) connected to a laser flash photolysis system (LP980, Edinburgh Instruments, Inc.), which has been previously described [34]. Kinetic traces were recorded in Argon-, air-, and oxygen-saturated solution, whereas transient absorbance spectra were only recorded in Argon-saturated acetonitrile. Data analysis was performed using Igor Pro 8 software. Stock solutions of **1** and **2** were prepared in acetonitrile so that the absorption at 266 or 308 nm was between 0.2 and 0.8.

2.5. Femtosecond and nanosecond transient absorption spectroscopy

Transient absorption spectroscopy was carried out using an integrated Helios and EOS experimental apparatus (Ultrafast Systems) with an ytterbium femtosecond laser (Hyperion; fundamental: 1030 nm, pulse duration: ~290 fs, repetition rate: 2.14 kHz (femtosecond experiments) or 1.0 kHz (nanosecond experiments)). The pump beam was generated using a three-stage optical parametric amplifier (Apollo-Y) with a pulse duration of 100–400 fs. The femtosecond broadband probe between 360 and 500 nm was generated using the second harmonic of the laser at 515 nm in a thin sapphire plate. A second broadband probe between 500 and 910 nm was generated using the laser fundamental in a 1 cm sapphire plate. Probe beams were directed through a Smart Delay Line to scan the time domain with a delay window of ~ 7.5 ns and a minimum step size of ~ 3 fs. The nanosecond probe was generated using a separate supercontinuum laser (MOPA-based; pulse duration: ~0.75 ns). The pump–probe delay was generated electronically in the

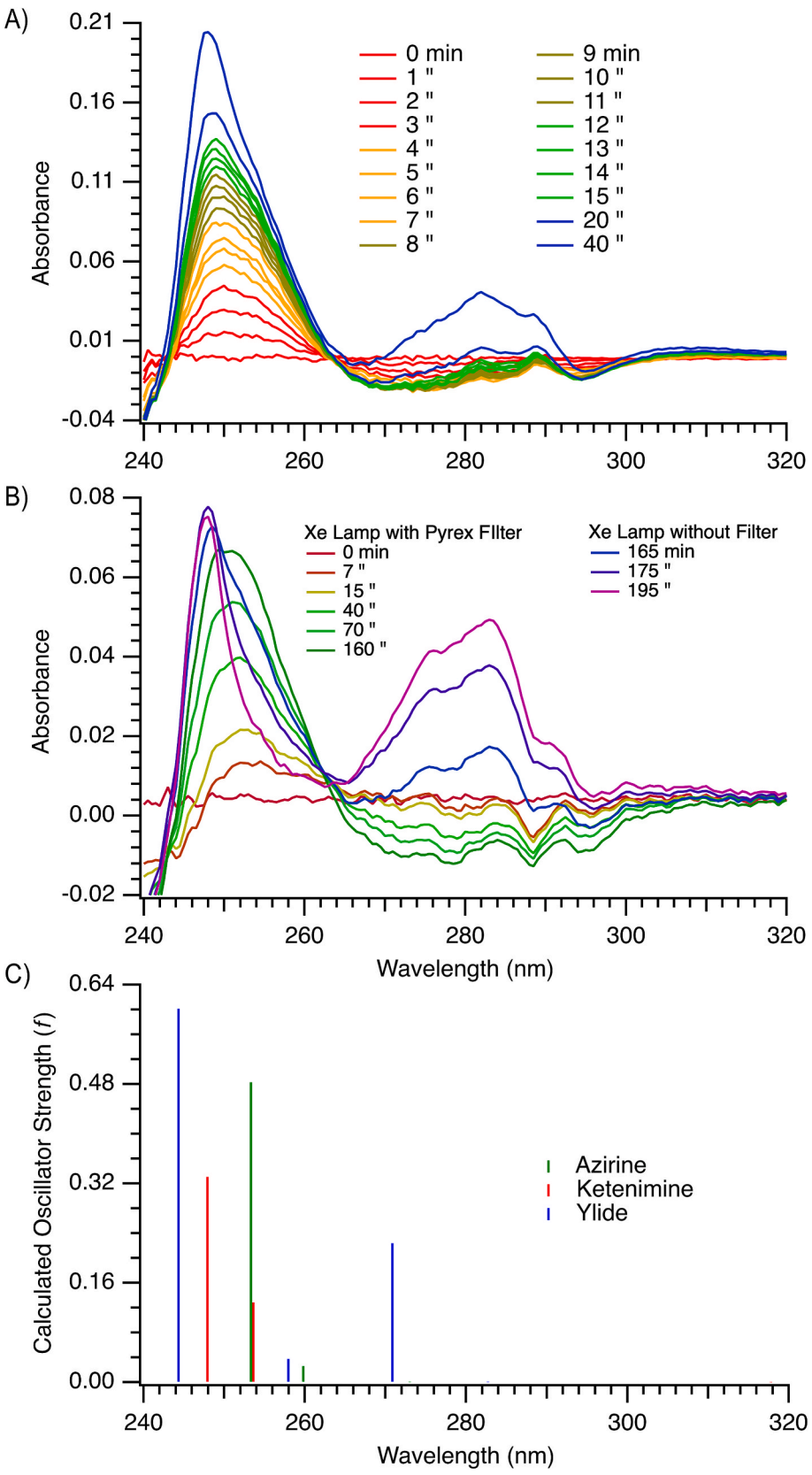

Fig. 5. A) Difference absorption spectra obtained by irradiating **1** in mTHF at 77 K with a Xe lamp without a quartz filter as a function of time. B) Difference absorption spectra obtained by irradiating **1** in mTHF at 77 K with a Xe lamp through a Pyrex filter for 160 min followed by irradiation through a quartz filter. C) TD-DFT (B3LYP/6–31+G(d)/CPCM/THF)-calculated electronic transitions for **2**, **3**, and **4**.

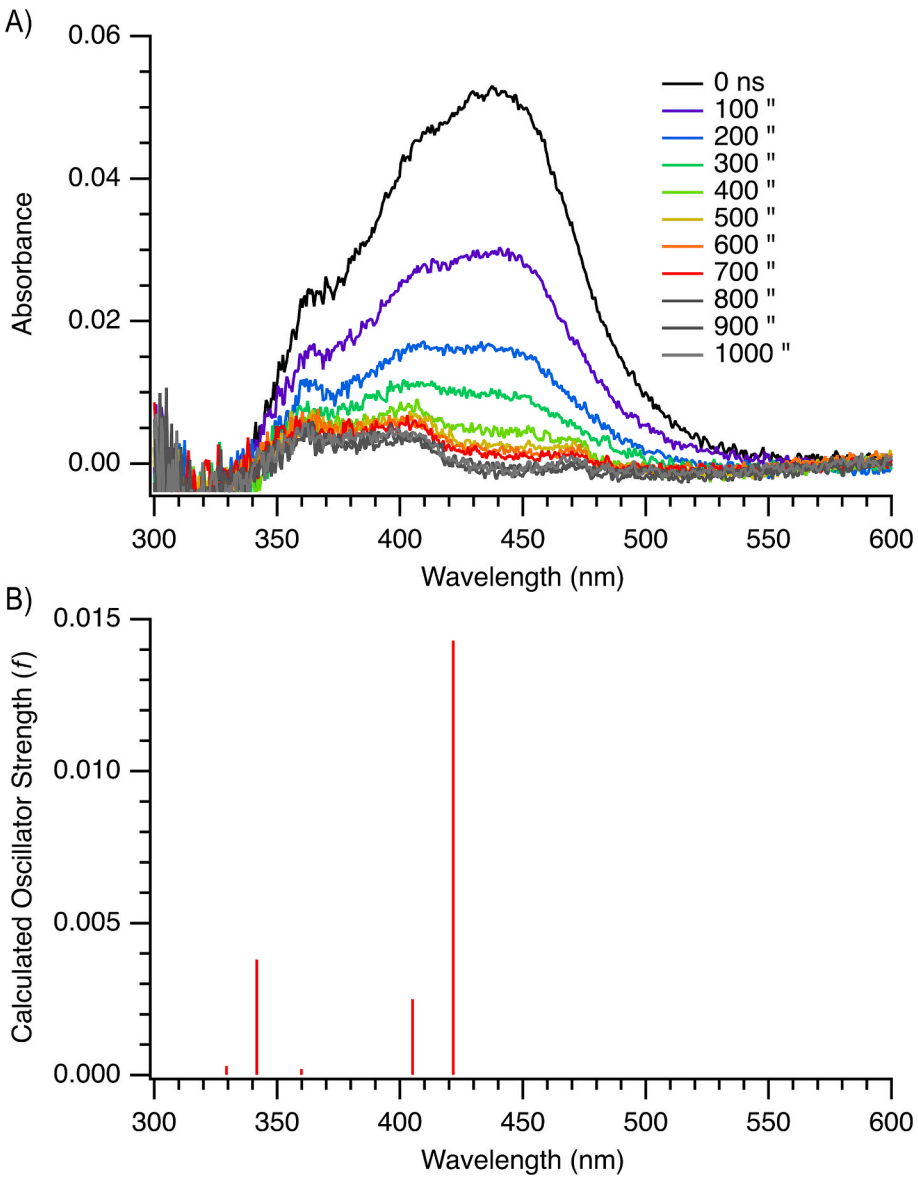

Fig. 6. A) Transient absorption spectra obtained by laser flash photolysis of **1** in argon-saturated acetonitrile at 308 nm. B) TD-DFT (B3LYP/6–31+G(d)/CPCM/acetonitrile)-calculated absorption spectrum of ^{3}**1N**.

nanosecond transient absorption experiments. All probes were split into two separate beams, one of which was directed onto the reference detector and the other through the sample compartment onto the signal detector. All samples were pumped with < 85 nJ at 470 nm. The samples were prepared in dichloromethane so that the optical density at 470 nm was 0.4–0.6 in a quartz cuvette with a 2 mm path length. Each solution was degassed using at least three freeze–pump–thaw cycles.

2.6. EPR spectroscopy

Frozen X-band EPR spectra were recorded at 5 K on a Bruker EMX EPR spectrometer with an ER-4116DM dual-mode resonator and an Oxford ESR900 flow cryostat, as described before.[35] mTHF solution of **1** (5 mM) and **2** (5 mM) were placed in a Wilmad Low Pressure/Vacuum Suprasil EPR tube and the sample was degassed by using the freeze–pump–thaw method. The solution formed a glassy matrix at 5 K in the EPR instrument. Calibration was performed at 9.390620 GHz, and the sample of **1** was irradiated with a 325 nm LED light for 45 min followed by 254 nm UV pen for 15 min, and sample of **2** was irradiated with 254 nm UV pen for 40 min.

2.7. Calculations

Geometry optimization was performed at the B3LYP/6–31+G(d) and B3PW91/6–311+G(d,p) levels of theory, as implemented in the Gaussian16 program [36–39]. The transition states were confirmed to have one imaginary vibrational frequency, and intrinsic reaction coordinate calculations were used to verify that the transition states corresponded to the expected reactant and product [10]. To obtain the calculated absorption spectra for triplet excited states and reactive intermediates, time-dependent density functional theory (TD-DFT) calculations were conducted at the same levels of theory with the same basis sets [34]. The B3LYP/6–31+G(d)-calculated IR bands were scaled by 0.9601 [40].

3. Results and discussion

3.1. Product studies

Irradiation of **1** in acetonitrile-d_3 with a 455 ± 10 nm LED resulted in the quantitative formation of **2**, as determined using ^{1}H NMR

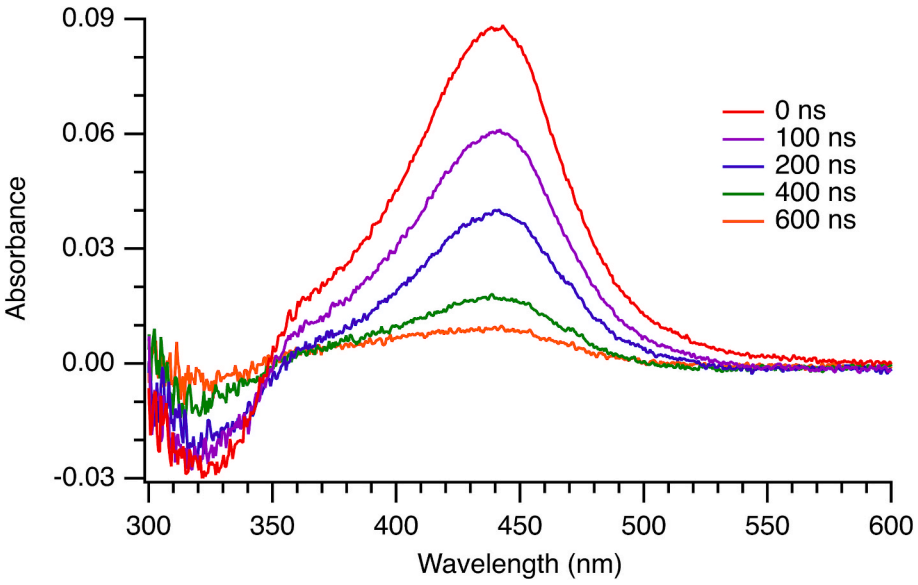

Fig. 7. Nano-second transient (ns-TA) absorption spectra obtained by laser flash photolysis of **2** in argon-saturated acetonitrile at 308 nm.

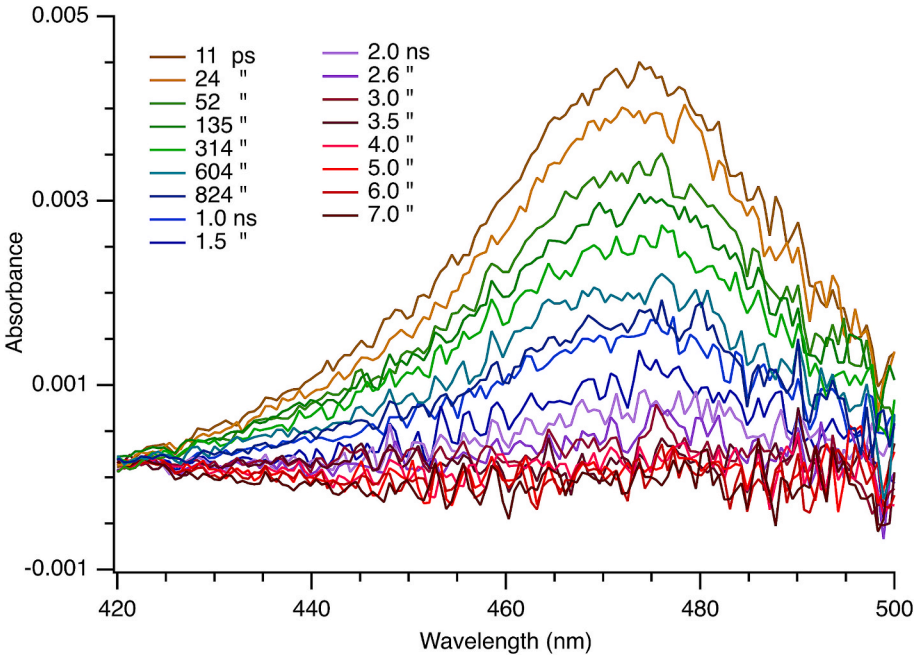

Fig. 8. Absorption spectra obtained by femto-second transient absorption spectroscopy of **1** in argon-saturated acetonitrile.

spectroscopy (Scheme 3). Irradiation of **2** in chloroform-*d* through a Pyrex filter did not yield any products (Scheme 3), whereas irradiation with a 254 nm UV pen depleted **2** and yielded the diaza-bicyclic product **5** (Scheme 4). For clarification, the absorption spectra of **1** and **2** are displayed in the SI (Figs. S1-S2).

The results from the present photochemical experiments are in agreement with the results of Padwa et al. [31,4], who first proposed that ylide **3** is formed from the S_1 of **1** and that heterocycle **5** is formed via a 1,3-dipolar addition between **3** and **2** [31]. However, these product studies do not establish whether the photoexcitation of **1** or **2** generates the corresponding singlet or triplet vinylnitrene (^{1}**1N** or ^{3}**1N**) or whether the photoreactivity occurs on the singlet or triplet surface.

In the current investigation, we theorized that the photoexcitation of **1** leads to the formation of a hot singlet state (S_1) of **1**, which decays to yield **2** and **4** in a concerted manner. However, we cannot rule out S_1 of **1** yielding ^{1}**1N**, which will subsequently form products **2** and **4** (Scheme 5). Furthermore, we expected that the S_1 of **1** may intersystem cross to the first triplet excited state (T_1) of **1** to yield ^{3}**1N**, which can potentially decay to form **2** and **4**. With the above postulation, we wanted to determine whether irradiation of **2** at longer wavelengths results in the formation of ^{3}**1N**.

3.2. *Irradiation of 1 and 2 in argon matrices*

We investigated whether the excitation of **1** and **2** yield the same product(s) in cryogenic argon matrices and if the different products would form depending on the irradiation wavelength. Azide **1** deposited in an argon matrix was first irradiated with a 325 nm laser then with a 254 nm UV pen. Matrix irradiation resulted in significant depletion of the IR bands of azide **1** at 2140, 2114, 1499, 1316, 1302, 1077, 910,

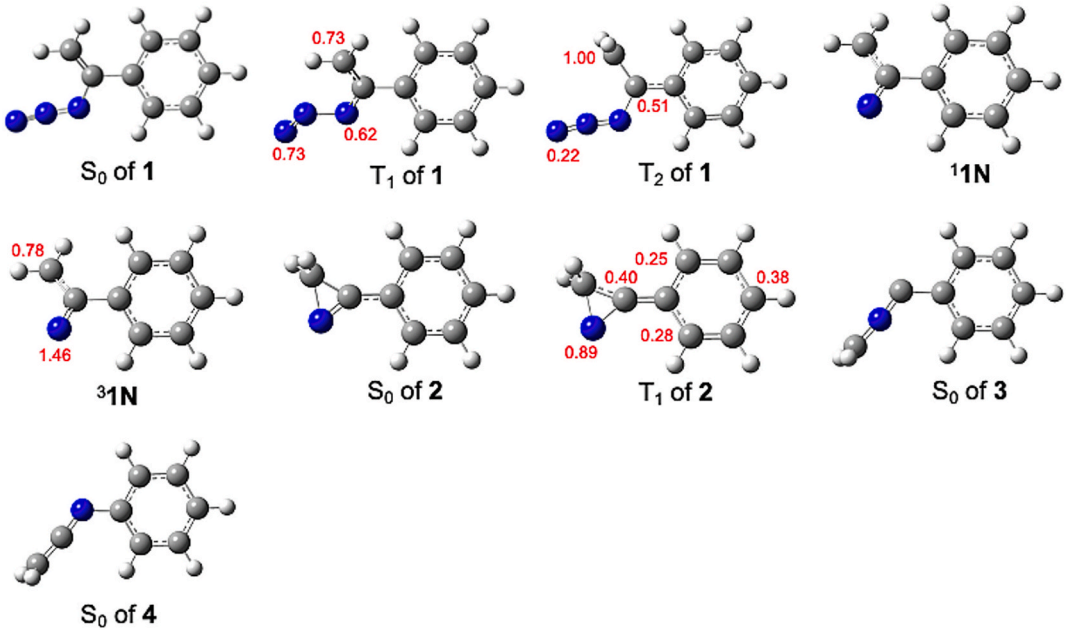

Fig. 9. Optimized (B3PW91/6–311+G(d,p)/CPCM/acetonitrile) structures of **1,** T_1 of **1**, T_2 of **1**, ^{3}**1N**, ^{1}**1N**, **2**, T_1 of **2, 3**, and **4**. The calculated spin densities are shown in red. (For interpretation of the references to colour in this figure legend, the reader is referred to the web version of this article.)

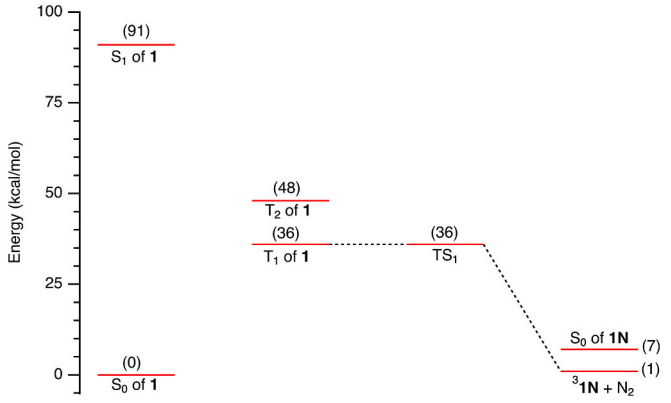

Fig. 10. Calculated (B3PW91/6–311+G(d,p)/CPCM/acetonitrile)) stationary points on the triplet surface of **1** for the formation of ^{3}**1N**. Energies are in kcal/mol.

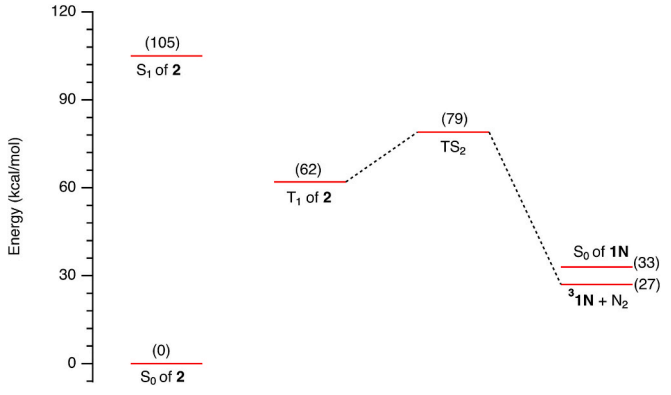

Fig. 11. Calculated (B3PW91/6–311+G(d)/CPCM/acetonitrile) stationary points on the triplet surface of **2** for the formation of ^{3}**1N**. Energies are in kcal/mol. The energy of T_1 of 2 is from its optimized structure.

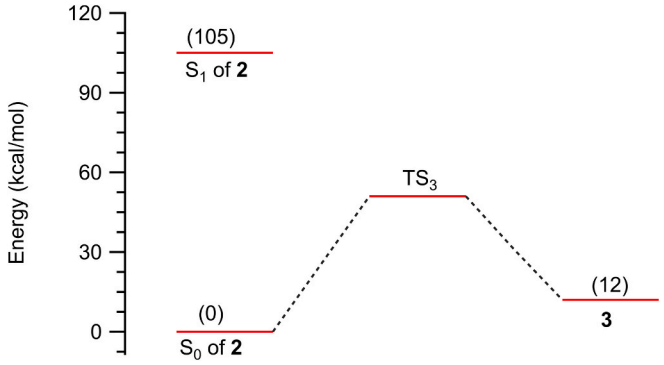

Fig. 12. Calculated (B3PW91/6–311+G(d)/CPCM/acetonitrile) stationary points on the surface of **2** for the formation of **3**. Energies are in kcal/mol. The energy of S_1 of **2** is from TD-DFT calculations.

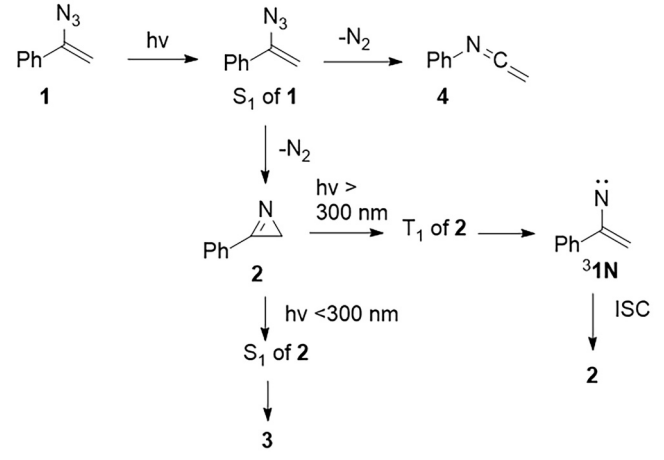

Scheme 6. Proposed mechanism for forming photoproducts **2**, **3**, and **4** upon excitation of 1 and 2 in acetonitrile and cryogenic matrices.

829, 770, 698, 656, and 606 cm^{-1} (Fig. S3) and the concurrent formation of new bands (See SI, Fig. S3). Specifically, significant new bands appeared at ~ 1755, 1752, 992, 762, 693, and 691 cm^{-1} after 45 min of irradiation at 325 nm (Fig. 1A and S4). These bands were assigned to product **2** by comparison to its observed and calculated (B3LYP/6–31 + G(d)) IR spectra (Fig. 1B). The broadness of the bands at ~ 1755, 1752, and 992 cm^{-1} is likely due to matrix splitting. As argon atoms freeze around the trapped molecule of interest, there may be multiple local minima for the arrangement of the argon atoms packed around the trapped species. Each local minimum will interact slightly differently with the trapped molecule, leading to slightly different infrared spectral bands. These are known as site split bands. The calculated and scaled bands for **2** are located at 1748 (107×10^{-40} esu^2 cm^2), 980 (152), 744 (243), 675 (70), and 671 (201) cm^{-1}. In addition, weak bands were observed at 2053 and 2032 cm^{-1} (Fig. 2A), which were assigned to **4** by comparison to its reported spectrum in an argon matrix, which has major bands at 2050, 2030, 1597, 1494, and 763 cm^{-1}, and its calculated and scaled IR spectrum (Fig. 2B) [27]. It should be noted that a small amount of **2** formed upon deposition of **1** in the matrix, but these bands grew further following irradiation.

Further irradiation of the matrix with the 254 nm UV pen yielded new bands at 2053, 2033, 1928, 1905, 1892, 1457, 1449, 1269, 1115, 1073, 788, 682, 688, and 605 cm^{-1} (Fig. 3A and S5-8). The bands at 2053 and 2033 cm^{-1} were assigned to **4**, whereas those at 1928, 1905, 1892, 1457, 1449, 1269, 1115, 1073, 788, 682, 688, and 605 cm^{-1} were assigned to **3**. These assignments are in agreement with previously published IR spectra of **3** and **4** in argon matrices and are further supported by comparison to their calculated and scaled spectra (Fig. 3B and Figs. S4-S9) [27]. It should be noted that the intensity of bands corresponding to **2** grew further upon continued irradiation at 254 nm.

To verify that products **4** and **2** were generated from azide **1** and that product **3** can be obtained from **2**, we irradiated **2** in an Argon matrix. Azirine **2** deposited in an Argon matrix at 14 K was irradiated with a 325 nm laser for 1 h, but no new IR bands were formed. Subsequent irradiation with a 254 nm UV pen for 30 min resulted in significant depletion of the IR bands of azirine **2** at 1752, 1457, 1328, 988, 760, 690, and 534 cm^{-1} (Fig. 4 and Fig. S9). Concurrently, new bands formed at 1925, 1900, 1885, 1580, 1495, 1114, 1073, 782, 770, 693, 678, 668, 619, and 602 cm^{-1}, which were assigned to **3** [4,5]. The bands at ~ 1900, 1885, and 1880 cm^{-1} were attributed to matrix splitting. Further irradiation resulted in complete depletion of the IR bands of **2** and an increase in the intensity of the IR bands of **3**.

Further, the irradiation of **2** at 325 nm in Argon matrices does not yield any new photoproducts, whereas irradiation at shorter wavelengths gives **3**. In contrast, irradiation of **1** at 325 nm results in **2** and **4** as the major and minor products, respectively, whereas irradiation at 254 nm yields **2**, **3**, and **4**. Because **4** is not formed upon irradiation of **2** at 254 nm, we conclude that **4** is only formed from azide **1** (Scheme 5). We also attempted to identify the IR bands that correspond to ^{3}**1N** (see Fig. S10, 1437 (48×10^{-40} esu^2 cm^2), 1213 (79), and 739 (403) cm^{-1}), but could not unambiguously assign any major bands to its formation.

3.3. UV absorption in cryogenic matrices

To further confirm that photochemical transformation of **1** can result in the formation of **2**, we irradiated **1** in glassy mTHF at 77 K. The differentiated or time-resolved absorption spectra were obtained by subtracting the spectra of the irradiated matrix from that of the initial sample of **1** (Fig. 5A and 5B). Irradiation of **1** with a Xe lamp through a quartz filter produced a new absorption band centered at 252 nm (Fig. S11). We assigned this band to product **2** by comparison to its published UV spectrum [41] and TD-DFT (6–31+G(d)/CPCM/THF)-calculated spectrum (Fig. 5C), in which the major electronic transition is located at 253 nm ($f = 0.4797$). This band grew upon further irradiation, but prolonged irradiation resulted in a new less intense band at 283 nm, a shift of the band at 252 nm to 248 nm, and depletion of the bands at ~ 272 and ~ 295 nm. We assigned the bands at 248 and 283 nm to **3** by comparison to the reported spectrum, which has major absorption bands at ~ 230 and 280 nm and a weaker band at ~ 380 nm [42]. This assignment was further supported by the TD-DFT (6–31+G(d)/CPCM/THF)-calculated spectrum of **3**, in which the major electronic transitions are located at 244 nm ($f = 0.5981$), 257 nm ($f = 0.0365$), and 272 nm ($f = 0.2323$) with a weaker transition at 423 nm ($f = 0.0023$) (Fig. 5C).

In another experiment, irradiation of **1** in a glassy mTHF matrix with a Xe lamp through a Pyrex filter resulted in the formation of a band with λ_{max} at 252 nm (Fig. 5C), which was assigned to **2**, as discussed above. After removal of the Pyrex filter, further matrix irradiation through a quartz filter caused the absorption band of **2** at 252 nm to shift to 248 nm with the concurrent formation of a new band at 283 nm, and these band were assigned to **3**, as before. Thus, we confirmed that initially formed **2** is converted to **3** upon irradiation through a quartz filter. The formation of **4** in glassy mTHF is also possible because its TD-DFT (6–31+G(d)/CPCM/THF)-calculated spectrum has major electronic transitions at 318 nm ($f = 0.0002$), 253 nm ($f = 0.126$), 248 nm ($f = 0.335$), and 213 nm ($f = 0.1459$) (Fig. 5C). In addition, a weak absorption band was observed between 320 and 420 nm (Fig. S11). Although the TD-DFT (6–31+G(d)/CPCM/THF)-calculated spectrum of ^{3}**1N** exhibits an electronic transition at 420 nm ($f = 0.014$) (Fig. S12), the observed band could not be assigned to ^{3}**1N** because **4** and **3** also have calculated absorption bands at wavelengths above 400 nm.

The above result suggests that, in glassy mTHF, irradiation of azide **1** at wavelengths above 300 nm results in the formation of **2**, whereas irradiation at shorter wavelengths yields **3** from **2**. However, the formation of ^{3}**1N** or **4** in cryogenic mTHF matrices from the irradiation of **1** could not be established.

3.4. Nanosecond laser flash photolysis

Nanosecond laser flash photolysis was used to investigate whether **1** or **2** forms triplet vinylnitrene ^{3}**1N** in solution. Laser flash photolysis of **1** in argon-saturated acetonitrile at 308 nm resulted in a transient absorption spectrum with λ_{max} at 437 nm and a smaller absorption band at 364 nm (Fig. 6A). The transient absorption corresponds well to the TD-DFT-calculated spectrum of ^{3}**1N** (Fig. 6B), which has a major electronic transition at 422 nm ($f = 0.014$). In argon-saturated acetonitrile, the lifetime of ^{3}**1N** was 190 ns ($k = 5.26 \times 10^6$ s^{-1}), whereas the lifetime became shorter in oxygen-saturated acetonitrile (140 ns, $k \sim 7.14 \times 10^6$ s^{-1}; Fig. S13). Rate constants of 7–20 $\times 10^8$ M^{-1} s^{-1} have been reported for the reaction of triplet vinylnitrenes with oxygen [19]. As the concentration of oxygen in oxygen-saturated acetonitrile has been estimated to be 0.0091 M [43], the rate constant of ^{3}**1N** reacting with oxygen was calculated to be 7.9×10^8 $M^{-1}s^{-1}$, which further supports the assignment of the transient absorption to ^{3}**1N**.

It should be noted that the transient absorption spectra obtained by laser flash photolysis of **1** at 308 nm exhibit residual absorption between 350 and 400 nm, indicating the formation of **3**. Thus, we theorized that during laser flash photolysis of **1** at 308 nm, **2** forms within the laser pulse (17 ns) and the transient absorption originates from secondary irradiation of **2**, which yields ^{3}**1N**.

Laser flash photolysis of azide **1** at 266 nm did not yield any significant absorption on short timescales. However, on a microsecond timescale, a weak transient absorption was observed between 300 and 400 nm that did not decay significantly (Fig. S14). We assigned this transient to intermediate **3** by comparison to its reported transient absorption spectra.[40] As mentioned above, **2** could form (from **1**) with a kinetic shorter than the pulse width of the laser. However, further irradiation of the sample would form intermediate **3**, as illustrated in Scheme 4.

To further support the formation of **2** from **1** within the laser pulse and investigate the wavelength-dependent photochemistry of **2**, we carried out laser flash photolysis of **2** at both 308 and 266 nm. On shorter timescales (nano-second), the transient absorption spectra

obtained by laser flash photolysis of **2** at 308 nm (Fig. 7) were similar to those obtained by laser flash photolysis of **1** using the same laser (Fig. 6). Similar transient absorption spectra were obtained in dichloromethane and mTHF (Fig. S15). Therefore, we conjecture that the photoexcitation of **2** at 308 nm yields ^{3}**1N**. In contrast, laser flash photolysis of **2** at 266 nm yielded a weak transient absorption that was assigned to the spectrum of intermediate **3** (Fig. S16).

3.5. Ultrafast transient absorption spectroscopy (fs-TA & ns-TA)

To identify the S_1 transient of **1** and confirm that the irradiation of **1** does not yield ^{3}**1N**, we carried out the fs-TA of **1**. Photoexcitation at 340 nm of **1** in Argon-saturated acetonitrile resulted in a broad transient absorption band between 420 to 500 nm centered at ca. 473 nm (Fig. 8). Since this transient was short-lived (22 ps; Fig. S18), we assigned it to the S_1 of **1** or vinylnitrene ^{1}**1N**. However, the TD-DFT (B3LYP/6–31 + G (d)/CPCM/acetonitrile)-calculated absorption spectrum of ^{1}**1N**, which has major electronic transitions at 539 nm (f = 0.0005), 442 nm (f = 0.0091), 389 nm (f = 0.0126), and 359 nm (f = 0.0026) (Fig. S19), did not agree well with the observed transient absorption. Similarly, the calculated spectra of T_2 of **1**, T_1 of **1**, and T_1 of **2** did not correspond to the observed spectra (Fig. S20–S22). Thus, we cautiously assigned this transient to S_1 of **1**, which must decay by extruding a N_2 molecule to form **2**. We cannot exclude that ^{1}**1N** forms a hot excited state, and the TD-DFT calculations for modeling the absorption spectrum for ^{1}**1N** is not very accurate.

3.6. EPR spectroscopy

Irradiation of **1** and **2** in degassed mTHF matrices at 5 K did not result in any EPR signals that can be assigned to formation of ^{3}**1 N** (see Fig. S34). However, it should be noted that triplet vinylnitrenes are not stable at cryogenic temperatures unless they are part of a cyclic structure that prevents rotation of the vinylic C=C-N moiety.[17,18,26] In contrast, flexible triplet vinylnitrenes intersystem cross to stable products at cryogenic temperature.[10,16,19].

3.7. Calculations

To support the proposed reaction mechanism for photoproduct formation from **1** and **2**, DFT c alculations were performed using both B3LYP/6–31+G(d) and B3PW91/6–31+G(d), as implemented in Gaussian16 [36–39]. The IR and UV spectra were calculated using B3LYP/6–31+G(d) to allow comparisons with our studies on 2-azidovinylbenzene and 2-phenyl-*2H*-azirine in cryogenic matrices [10].

The stationary points on the reaction surfaces of **1** and **2** were calculated using B3PW91/6–311 + G(d,p))/CPCM/acetonitrile. The optimized structures of **1**, T_1 of **1**, T_2 of **1**, ^{3}**1 N**, ^{1}**1 N**, **2**, T_1 of **2**, **3**, and **4** are displayed in Fig. 9, with the calculated spin densities for T_2 of **1**, T_1 of **1**, ^{3}**1 N**, and T_1 of **2** shown in red. The T_1 of **1** is best described as having the unpaired electrons located mainly on the vinyl azido chromophore, with spin densities of 0.62 and 0.73 on the N_α and N_β atoms, respectively, and a spin density of 0.73 on the C_β atom (Fig. 9). In contrast, the T_2 of **1** can be described as a 1,2-biradical, as the vinylic C_α and C_β atoms have spin densities of 0.51 and 1.00, respectively. We plotted stationary points on the triplet surface for both **1** and **2** (Figs. 10 and 11). Based on TD-DFT calculations for the optimized structure of the singlet ground state (S_0) of **1**, S_1 of **1** is located 91 kcal/mol above S_0 (Fig. 10). Importantly, the calculated transition state barrier for T_1 of **1** to form ^{3}**1 N** (36 kcal/mol) is similar in energy to the T_1 of **1**, indicating that the dissociation of T_1 of **1** to form ^{3}**1 N** and a N_2 molecule is an almost barrierless process. The computational investigations established that the formation of ^{3}**1 N** from **1** is not feasible since the direct irradiation of **1** cannot produce the expected triplet manifold of **1**.

We used Noodleman's broken symmetry method to optimize the structure of ^{1}**1N** [44]. The singlet configuration of ^{1}**1N** is located 7 kcal/mol above the triplet configuration. However, as there is significant spin contamination from the triplet ($<S^2> = 1.0109$), this calculation does not accurately estimate the energy gap. Qian et al. estimated an energy gap of 15.2 kcal/mol between singlet and triplet vinylnitrene CH_2=CH–N using the CASPT2(6,5)/cc-pVDZ//CASSCF(6,5)/cc-pVDZ level of theory. Despite the phenyl substitution, **1N** is reasonably expected to have a similar energy gap [25].

TD-DFT calculations locate S_1 of **2** and T_1 of **2** at 105 and 70 kcal/mol above its S_0, respectively, whereas the optimized structure of T_1 of **2** is at ca. 62 kcal/mol above its S_0. The calculated transition state barrier to form ^{3}**1 N** from T_1 of **2** is 17 kcal/mol (Fig. 11). However, the optimized energy of T_1 of **2** is likely underestimated and closer to the TD-DFT-calculated energy. Thus, cleavage from T_1 of **2** to form ^{3}**1 N** is feasible in solution and matrices. Finally, we optimized the transition state barrier for **2** forming **3**. This barrier is located 51 kcal/mol above the S_0 of **2**, and thus it is feasible for vibrationally hot **2** to form **3** (Fig. 12).

4. Conclusion

Ultrafast transient absorption spectroscopy of **1** in acetonitrile revealed the formation of a short-lived transient (τ = 22 ps, λ_{max} at 472 nm), which was assigned to the S_1 of **1** rather than ^{1}**1N** (Scheme 6). However, multireference calculations are needed to further support this assignment. In addition, we confirmed that the S_1 of **1** does not intersystem cross to its triplet manifold to yield ^{3}**1N**. Instead, it theorized that the S_1 of **1** decays to form **2** in a concentrated manner. Similarly, **4** is expected to form from the S_1 of **1**. We concluded that the large singlet–triplet energy gap for **1** prevents intersystem crossing to the between the singlet and triplet surfaces of **1**. In contrast, the irradiation of **2** at wavelengths above 300 nm resulted in the formation of ^{3}**1N**, which decayed to re-form **2** in acetonitrile and cryogenic matrices. Thus, ^{3}**1N** is not the precursor of **4** in cryogenic matrices. The photoreactivity of **2** is not significantly affected by the reaction medium or temperature because the intersystem crossing of ^{3}**1N** is not restricted by either temperature or medium.

CRediT authorship contribution statement

W.Dinindu Mendis: Writing – original draft, Supervision, Investigation. **Abdelqader M. Jamhawi:** Investigation. **Rajkumar Merugu:** Investigation. **Dmitrii Govorov:** Conceptualization. **Katrin H. Vilinsky:** Investigation. **Bakar Alomari:** Investigation. **Bruce S. Ault:** Investigation. **A.Jean-Luc Ayitou:** Writing – review & editing, Investigation. **Anna D. Gudmundsdottir:** Writing – review & editing, Validation, Supervision.

Declaration of competing interest

The authors declare that they have no known competing financial interests or personal relationships that could have appeared to influence the work reported in this paper.

Acknowledgment

This work was supported by the NSF grants (CHE-2400277 awarded to ADG and CHE-2247930 awarded to AJA). The authors thank the Ohio Supercomputer Center (PES0597) and ACCESS (PSC at Bridges-2 RM, CHE240153) for allocating computing resources used in this investigation. BA is grateful for support from the ACS SEED program and WDM and RM for Doctoral Enhancement Funding from the Chemistry Department at the University of Cincinnati.

Appendix A. Supplementary data

Supplementary data to this article can be found online at https://doi.org/10.1016/j.jphotochem.2025.116427.

Data availability

Data will be made available on request.

References

[1] N. Thirupathi, F. Wei, C.-H. Tung, Z. Xu, Divergent synthesis of chiral cyclic azides via asymmetric cycloaddition reactions of vinyl azides, Nat. Commun. 10 (2019) 3158, https://doi.org/10.1038/s41467-019-11134-8.

[2] F. Xu, F.-W. Zeng, W.-J. Luo, S.-Y. Zhang, J.-Q. Huo, Y.-P. Li, *2H*-Azirines: Recent progress in synthesis and applications, Eur. J. Org. Chem. 27 (2024) e202301292, https://doi.org/10.1002/ejoc.202301292.

[3] H. Hayashi, A. Kaga, S. Chiba, Application of vinyl azides in chemical synthesis: A recent update, J. Org. Chem. 82 (2017) 11981–11989, https://doi.org/10.1021/acs.joc.7b02455.

[4] J. Fu, G. Zanoni, E.A. Anderson, X. Bi, -Substituted vinyl azides: An emerging functionalized alkene, Chem. Soc. Rev. 46 (2017) 7208–7228, https://doi.org/10.1039/C7CS00017K.

[5] B. Saxena, R.I. Patel, J. Tripathi, A. Sharma, Visible light-assisted chemistry of vinyl azides and its applications in organic synthesis, Org. Biomol. Chem. 21 (2023) 4723–4743, https://doi.org/10.1039/D3OB00588G.

[6] E.P. Farney, T.P. Yoon, Visible-light sensitization of vinyl azides by transition-metal photocatalysis, Angew. Chem. Int. Ed. Engl. 53 (2014) 793–797, https://doi.org/10.1002/anie.201308820.

[7] S. Malo, S. Santra, J. Saha, D. Ghosh, I. Das, External photocatalyst-free photocycloaddition between triplet vinylnitrenes with 1,3-biradical character and activated olefins under 420 nm LEDs, Chem. Comm. 60 (2024) 12545–12548, https://doi.org/10.1039/D4CC03484H.

[8] B.D. Fairbanks, L.J. Macdougall, S. Mavila, J. Sinha, B.E. Kirkpatrick, K.S. Anseth, C.N. Bowman, Photoclick chemistry: A bright idea, Chem. Rev. 121 (2021) 6915–6990, https://doi.org/10.1021/acs.chemrev.0c01212.

[9] G.S. Kumar, Q. Lin, Light-triggered click chemistry, Chem. Rev. 121 (2021) 6991–7031, https://doi.org/10.1021/acs.chemrev.0c00799.

[10] O. Osisioma, M. Chakraborty, B.S. Ault, A.D. Gudmundsdottir, Wavelength-dependent photochemistry of 2-azidovinylbenzene and 2-phenyl-*2H*-azirine, J. Mol. Struct. 1172 (2018) 94–101, https://doi.org/10.1016/j.molstruc.2018.04.042.

[11] U. Banerjee, K. Thenna-Hewa, A.D. Gudmundsdottir, Triplet vinylnitrenes, in: J. F. Liebman, A. Greer (Eds.), The Chemistry of Nitrogen-Rich Functional Groups: Patai's Chemistry of Functional Groups, John Wiley & Sons Ltd, 2019, pp. 161–198.

[12] S. Rajam, A.V. Jadhav, Q. Li, S.K. Sarkar, P.N.D. Singh, A. Rohr, T.C.S. Pace, R. Li, J.A. Krause, C. Bohne, B.S. Ault, A.D. Gudmundsdottir, Triplet sensitized photolysis of a vinyl azide: Direct detection of a triplet vinyl azide and nitrene, J. Org. Chem. 79 (2014) 9325–9334, https://doi.org/10.1021/jo501898p.

[13] G. Maier, C. Schmidt, H.P. Reisenauer, E. Endlein, D. Becker, J. Eckwert, B. H. Andes Jr., L.J. Schaad, Blausäure-N-methylid: Darstellung, spektroskopische Eigenschaften und seine Beziehung zu anderen C_2H_3N-isomeren, Chem. Ber. 126 (1993) 2337–2352, https://doi.org/10.1002/cber.19931261024.

[14] C. Wentrup, Carbenes and nitrenes: Recent developments in fundamental chemistry, Angew. Chem. Int. Ed. Engl. 57 (2018) 11508–11521, https://doi.org/10.1002/anie.201804863.

[15] D.W. Gamage, Q. Li, R.A.A.U. Ranaweera, S.K. Sarkar, G.K. Weragoda, P.L. Carr, A. D. Gudmundsdottir, Vinylnitrene formation from 3,5-diphenyl-isoxazole and 3-benzoyl-2-phenylazirine, J. Org. Chem. 78 (2013) 11349–11356, https://doi.org/10.1021/jo401819g.

[16] S. Rajam, R.S. Murthy, A.V. Jadhav, Q. Li, C. Keller, C. Carra, T.C.S. Pace, C. Bohne, B.S. Ault, A.D. Gudmundsdottir, Photolysis of (3-methyl-*2H*-azirin-2-yl)-phenylmethanone: Direct detection of a triplet vinylnitrene intermediate, J. Org. Chem. 76 (2011) 9934–9945, https://doi.org/10.1021/jo200877k.

[17] S.K. Sarkar, O. Osisioma, W.L. Karney, M. Abe, A.D. Gudmundsdottir, Using molecular architecture to control the reactivity of a triplet vinylnitrene, J. Am. Chem. Soc. 138 (2016) 14905–14914, https://doi.org/10.1021/jacs.6b05746.

[18] S.K. Sarkar, A. Sawai, K. Kanahara, C. Wentrup, M. Abe, A.D. Gudmundsdottir, Direct detection of a triplet vinylnitrene, 1,4-naphthoquinone-2-ylnitrene, in solution and cryogenic matrices, J. Am. Chem. Soc. 137 (2015) 4207–4214, https://doi.org/10.1021/jacs.5b00998.

[19] X. Zhang, S.K. Sarkar, G.K. Weragoda, S. Rajam, B.S. Ault, A.D. Gudmundsdottir, Comparison of the photochemistry of 3-methyl-2-phenyl-*2H*-azirine and 2-methyl-3-phenyl-2*H*-azirine, J. Org. Chem. 79 (2014) 653–663, https://doi.org/10.1021/jo402443w.

[20] A.K. Schrock, G.B. Schuster, Photochemistry of naphthyl and pyrenyl azides: Chemical properties of the transient intermediates probed by laser spectroscopy, J. Am. Chem. Soc. 106 (1984) 5234–5240, https://doi.org/10.1021/ja00330a033.

[21] E. Leyva, M.S. Platz, E. Moctezuma, Investigation of phenyl azide photochemistry by conventional and time-resolved spectroscopy. Elucidation of intermediates and reaction mechanisms, J. Photochem. Photobiol. 11 (2022) 100126, https://doi.org/10.1016/j.jpap.2022.100126.

[22] P.N.D. Singh, S.M. Mandel, J. Sankaranarayanan, S. Muthukrishnan, M. Chang, R. M. Robinson, P.M. Lahti, B.S. Ault, A.D. Gudmundsdóttir, Selective formation of triplet alkyl nitrenes from photolysis of β-azido-propiophenone and their reactivity, J. Am. Chem. Soc. 129 (2007) 16263–16272, https://doi.org/10.1021/ja077523s.

[23] V. Parasuk, C.J. Cramer, Multireference configuration interaction and second-order perturbation theory calculations for the $1^3A''$, $1^1A''$, and $1^1A'$ electronic states of vinylnitrene and vinylphosphinidene, Chem. Phys. Lett. 260 (1996) 7–14, https://doi.org/10.1016/0009-2614(96)00865-2.

[24] C. Bornemann, M. Klessinger, Conical intersections and photoreactions of *2H*-azirines, Chem. Phys. 259 (2000) 263–271, https://doi.org/10.1016/S0301-0104(00)00207-X.

[25] W. Qian, P.R. Schreiner, A. Mardyukov, Preparation and photochemistry of parent triplet vinylarsinidene, J. Am. Chem. Soc. 146 (2024) 930–935, https://doi.org/10.1021/jacs.3c11432.

[26] D.M. Gatlin, W.L. Karney, M. Abe, B.S. Ault, A.D. Gudmundsdottir, Formation and reactivity of triplet vinylnitrenes as a function of ring size, J. Org. Chem. 84 (2019) 9215–9225, https://doi.org/10.1021/acs.joc.9b01191.

[27] E. Orton, S.T. Collins, G.C. Pimentel, Molecular structure of the nitrile ylide derived from 3-phenyl-*2H*-azirine in a nitrogen matrix, J. Phys. Chem. 90 (1986) 6139–6143, https://doi.org/10.1021/j100281a018.

[28] L. Xiang, Y. Niu, X. Pang, X. Yang, R. Yan, I_2-catalyzed synthesis of substituted imidazoles from vinyl azides and benzylamines, Chem. Comm. 51 (2015) 6598–6600, https://doi.org/10.1039/C5CC01155H.

[29] N.S.Y. Loy, S. Kim, C.-M. Park, Synthesis of unsymmetrical pyrazines based on α-diazo oxime ethers, Org. Lett. 17 (2015) 395–397, https://doi.org/10.1021/ol5034173.

[30] X. Li, S. Liao, Z. Wang, L. Zhang, Ligand-accelerated gold-catalyzed addition of in situ generated hydrazoic acid to alkynes under neat conditions, Org. Lett. 19 (2017) 3687–3690, https://doi.org/10.1021/acs.orglett.7b01359.

[31] A. Padwa, M. Dharan, J. Smolanoff and S. I. Wetmore. Photochemical transformations of small ring heterocyclic compounds. XLVII. Electronic details of the photocycloaddition of arylazirines. *J. Am. Chem. Soc.* 95 (1973), 1954-1961. DOI: 10.1021/ja00787a040.

[32] U. Banerjee, W.L. Karney, B.S. Ault, A.D. Gudmundsdottir, Photolysis of 5-azido-3-phenylisoxazole at cryogenic temperature: Formation and direct detection of a nitrosoalkene, *Molecules* 25 (2020) 543, https://doi.org/10.3390/molecules25030543.

[33] B.S. Ault, Infrared spectra of argon matrix-isolated alkali halide salt/water complexes, *J. Am. Chem. Soc.* 100 (1978) 2426–2433, https://doi.org/10.1021/ja00476a027.

[34] S.K. Sarkar, R.A.A. Upul Ranaweera, R. Merugu, N.M. Abdelaziz, J. Robinson, H. A. Day, J.A. Krause, A.D. Gudmundsdottir, Comparison of the photochemistry of acyclic and cyclic 4-(4-methoxy-phenyl)-4-oxo-but-2-enoate ester derivatives, J. Phys. Chem. A 124 (2020) 7346–7354, https://doi.org/10.1021/acs.jpca.0c04319.

[35] N. Ahmed, J.P.K. Kavikarage, D.F. Judkins, W.D. Mendis, R. Merugu, J.A. Krause, B.S. Ault, A.D. Gudmundsdottir, Unraveling the solid-state photoreactivity of carbonylbis(4,1-phenylene)dicarbonazidate with laser flash photolysis, J. Phys. Chem. A 127 (2023) 9705–9716, https://doi.org/10.1021/acs.jpca.3c04867.

[36] M.J. Frisch, G.W. Trucks, H.B. Schlegel, G.E. Scuseria, M.A. Robb, J.R. Cheeseman, G. Scalmani, V. Barone, G.A. Petersson, H. Nakatsuji, X. Li, M. Caricato, A.V. Marenich, J. Bloino, B.G. Janesko, R. Gomperts, B. Mennucci, H.P. Hratchian, J.V. Ortiz, A.F. Izmaylov, J.L. Sonnenberg, D. Williams-Young, F. Ding, F. Lipparini, F. Egidi, J. Goings, B. Peng, A. Petrone, T. Henderson, D. Ranasinghe, V.G. Zakrzewski, J. Gao, N. Rega, G. Zheng, W. Liang, M. Hada, M. Ehara, K. Toyota, R. Fukuda, J. Hasegawa, M. Ishida, T. Nakajima, Y. Honda, O. Kitao, H. Nakai, T. Vreven, K. Throssell, J.A. Montgomery, Jr., J.E. Peralta, F. Ogliaro, M.J. Bearpark, J.J. Heyd, E.N. Brothers, K.N. Kudin, V.N. Staroverov, T.A. Keith, R. Kobayashi, J. Normand, K. Raghavachari, A.P. Rendell, J.C. Burant, S.S. Iyengar, J. Tomasi, M. Cossi, J.M. Millam, M. Klene, C. Adamo, R. Cammi, J.W. Ochterski, R.L. Martin, K. Morokuma, O. Farkas, J.B. Foresman, D.J. Fox, Gaussian, Inc., Wallingford CT, 2016.

[37] C. Lee, W. Yang, R.G. Parr, Development of the Colle-Salvetti correlation-energy formula into a functional of the electron density, PhysRevB 37 (1988) 785–789, https://doi.org/10.1103/PhysRevB.37.785.

[38] J.-D. Chai, M. Head-Gordon, Long-range corrected hybrid density functionals with damped atom–atom dispersion corrections, PCCP 10 (2008) 6615–6620, https://doi.org/10.1039/B810189B.

[39] A.D. Becke, Density-functional thermochemistry. III. The role of exact exchange, J. Chem. Phys. 98 (1993) 5648–5652, https://doi.org/10.1063/1.464913.

[40] M. D. Halls, J. Velkovski and H. B. Schlegel. Harmonic frequency scaling factors for Hartree-Fock, S-VWN, B-LYP, B3-LYP, B3-PW91 and MP2 with the Sadlej pVTZ electric property basis set. Theor. Chem. Acc. 105 (2001), 413-421. DOI:.

[41] G. Smolinsky, Formation of azacyclopropenes by pyrolysis of vinyl azides, J. Org. Chem. 27 (1962) 3557–3559, https://doi.org/10.1021/jo01057a037.

[42] E. Albrecht, J. Mattay, S. Steenken, [3 + 2] cycloadditions and protonation by alcohols of photochemically generated nitrile ylides from *2H*-azirines. Formation and reactivities of azaallenium cations, J. Am. Chem. Soc. 119 (1997) 11605–11610, https://doi.org/10.1021/ja971648n.

[43] R. Battino. Oxygen and Ozone; Solubility Data Series, Vol. 7, Pergamon, Oxford, 1981.

[44] L. Noodleman, E.J. Baerends, Electronic structure, magnetic properties, ESR, and optical spectra for 2-Fe ferredoxin models by LCAO-X_α Valence bond theory, J. Am. Chem. Soc. 106 (1984) 2316–2327, https://doi.org/10.1021/ja00320a017.

Glossary

DFT: density functional theory
IR: infrared
mTHF: methyltetrahydrofuran
S_0: singlet ground state

S_1: first singlet excited state
T_1: first triplet exited state
T_2: second triplet excited state
TD-DFT: time-dependent density functional theory